Neuron, Volume *102*

Supplemental Information

Neocortical Projection Neurons Instruct Inhibitory Interneuron Circuit Development in a Lineage-Dependent Manner

Jason C. Wester, Vivek Mahadevan, Christopher T. Rhodes, Daniela Calvigioni, Sanan Venkatesh, Dragan Maric, Steven Hunt, Xiaoqing Yuan, Yajun Zhang, Timothy J. Petros, and Chris J. McBain

Wester et al 2019

Neocortical projection neurons instruct inhibitory interneuron circuit development in a lineage dependent manner

Supplemental Figures and Tables (Figures S1 – 8 and Tables S1 and 2; Table S3 is an Excel spreadsheet)

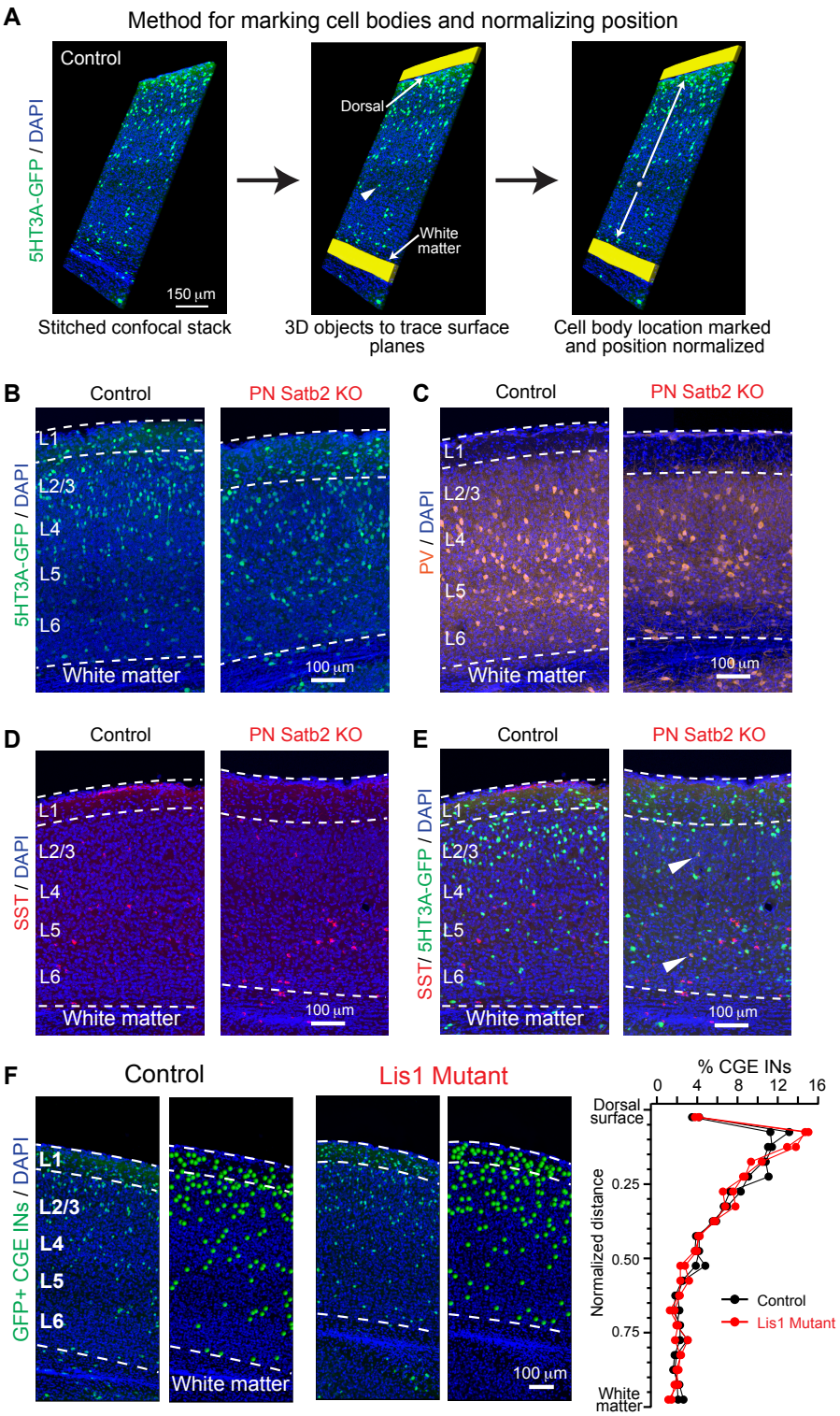

Figure S1. Related to Figure 2. Quantification of IN cell body positions from confocal stacks and confocal example images.

A) Schematic of method used to determine the normalized position of IN cell bodies relative to the dorsal cortical surface and white matter using Imaris software. Arrowhead indicates example cell.
B) Confocal images of 5HT3A-GFP+ INs used to mark cell body locations corresponding to examples in Figure 2A. Layers 1 – 6 are labeled in the control condition for reference.
C) Confocal images of PV IHC used to mark cell body locations of PV+ INs in Figure 2D.
D and E) Confocal images of SST IHC and overlaid 5HT3A-GFP signal used to mark cell body locations of SST+/GFP- INs in Figure 2G. White arrows indicate examples of SST+/GFP+ INs not counted in Figures 2G – I and K.
F) Examples of 5HT3A-GFP signal and cell body locations marked using Imaris software in control mice and Lis1 mutants. Histograms of the percentage of CGE INs as a function of normalized depth from the dorsal cortical surface (n = 2 mice/condition; 10 - 12 50 μm thick, 500 μm wide hemisphere sections/mouse).

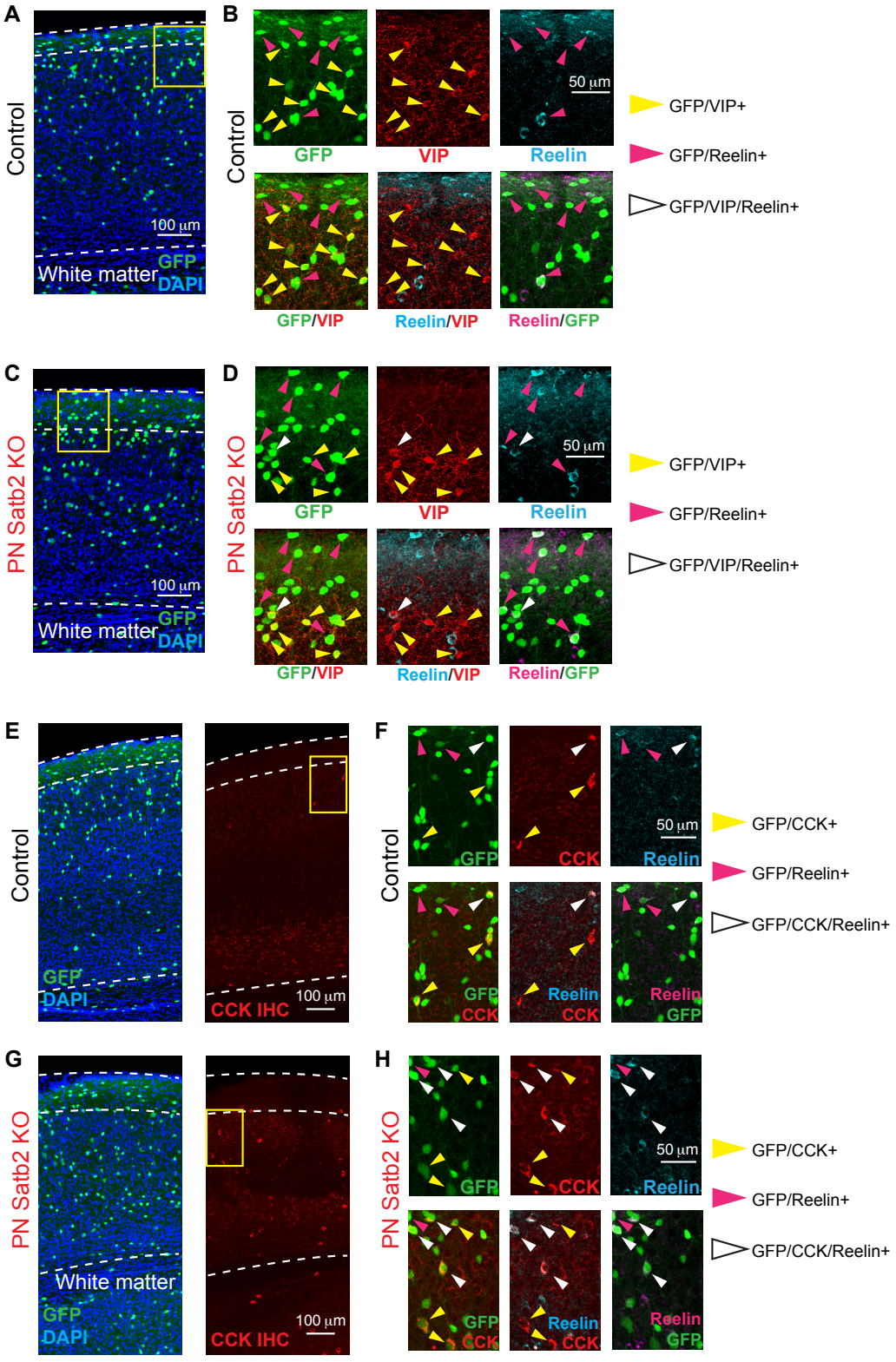

Figure S2. Related to Figure 3. IHC for VIP, reelin, and CCK.
A) 5HT3A-GFP signal for the control examples in Figures 3A and D. Yellow box indicates expanded region in (B).

B) Examples of co-immunostaining for VIP and reelin on the background of the 5HT3A-GFP signal. Signal and marker overlap were quantified throughout the entire section. Color channels have been pseudo-colored to more clearly show overlap of markers.
C) 5HT3A-GFP signal for the PN Satb2 KO example in Figure 3A and D. Yellow box indicates expanded region in (D).
D) Same as (B) for PN Satb2 KO example.
E) 5HT3A-GFP signal and CCK IHC used to mark cell bodies for the control section in Figure 3G. Yellow box indicates expanded region in (F).
F) Co-staining for CCK and reelin on the background of the 5HT3A-GFP signal. Signal and marker overlap were quantified throughout the entire section. Color channels have been pseudo-colored to more clearly show overlap of markers.
G) Same as (E) for PN Satb2 KO example.
H) Same as (F) for PN Satb2 KO example.

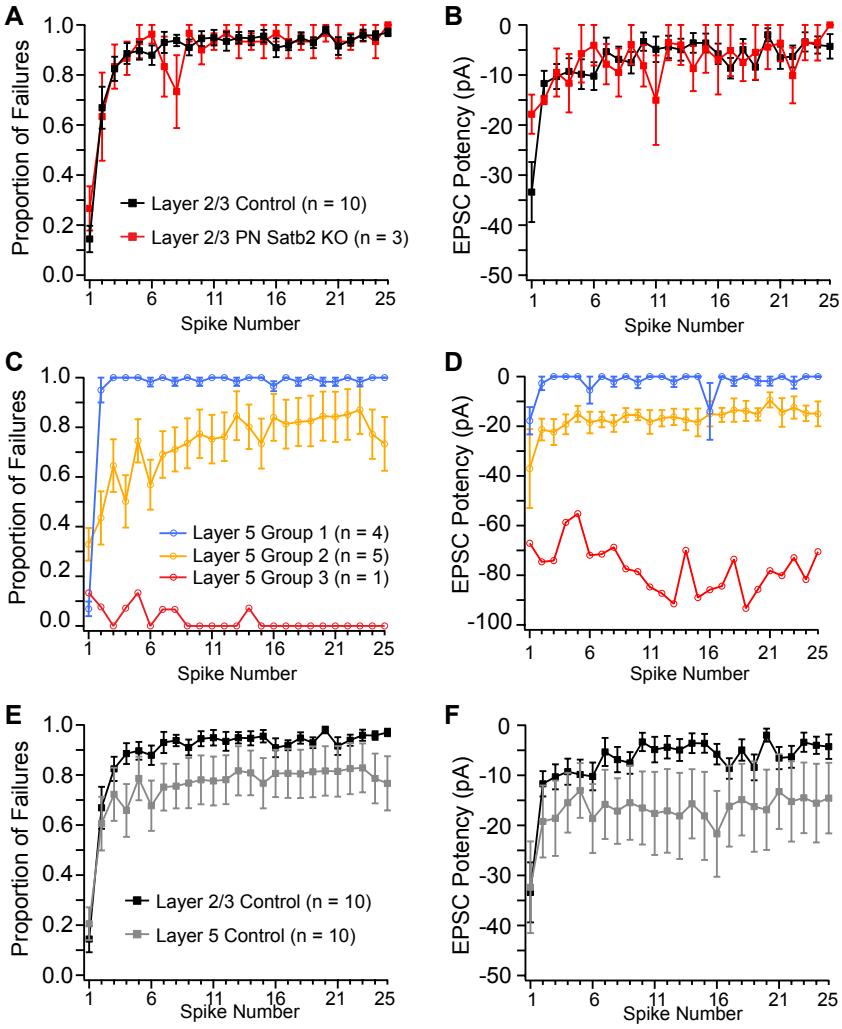

Figure S3. Related to Figures 4 and 5. Quantification of PN to IN synaptic properties from paired whole-cell recordings.

A) Proportion of failures for PN-to-IN synaptic connections in superficial cortex of control versus PN Satb2 KO mice during presynaptic action potential trains. Control, n = 10 synaptic connections; mutant, n = 3 synaptic connections.

B) EPSC potency related to (A).

C) Proportion of failures for PN-to-IN synaptic connections in deep layers of cortex in control mice, broken into three groups based on degree of synaptic depression. There was no correlation between the intrinsic membrane properties of the postsynaptic IN and group. Group 1: LS (1), CA – Linear (1), IS – Linear (2). Group 2: LS (2), CA – Linear (1), CA – Rectifying (1). Group 3: CA – Linear (1).

D) EPSC potency related to (C).

E) Proportion of failures for PN-to-IN synaptic connections during presynaptic action potential trains in superficial versus deep layers of cortex in control mice. Note higher variance for deep layer recordings. Superficial cortex (control), n = 10 synaptic connections; Deep cortex (control), n =11 synaptic connections.

F) EPSC potency related to (E).

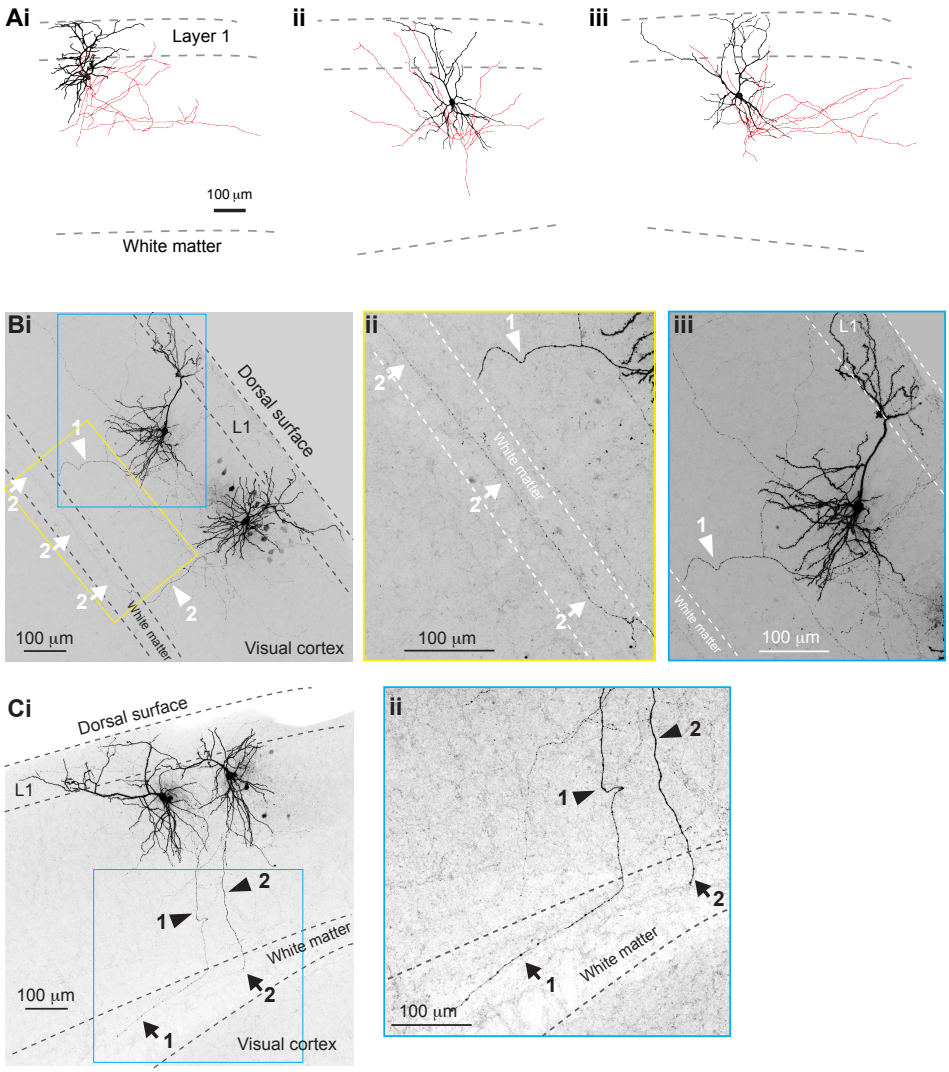

Figure S4. Related to Figure 4. Examples of PN morphologies in superficial cortex after loss of Satb2.

A) Reconstructions of PNs in Satb2 KO mice. Dendrites and soma are black and the axon is red. Note extensive axon collaterals in superficial cortex.

B) Primary axons were often observed entering the white matter in our sections (12/19 cells) (i) Example confocal image of two biocytin-filled PNs after loss of Satb2. Arrows highlight the primary axons of both cells descending towards white matter. Arrowheads denote the primary axon of cell 2 as it enters and projects through the white matter. (ii) Expansion of axon from cell 2 projecting through white matter. (iii) Expansion of cell 1 to highlight local axons projecting within superficial layers.

C) (i) Two additional examples of Satb2 KO PNs with axons descending towards and entering white matter. Arrows denote primary axons descending towards and then projecting through the white matter (arrowheads). (ii) Expansion of axons entering white matter.

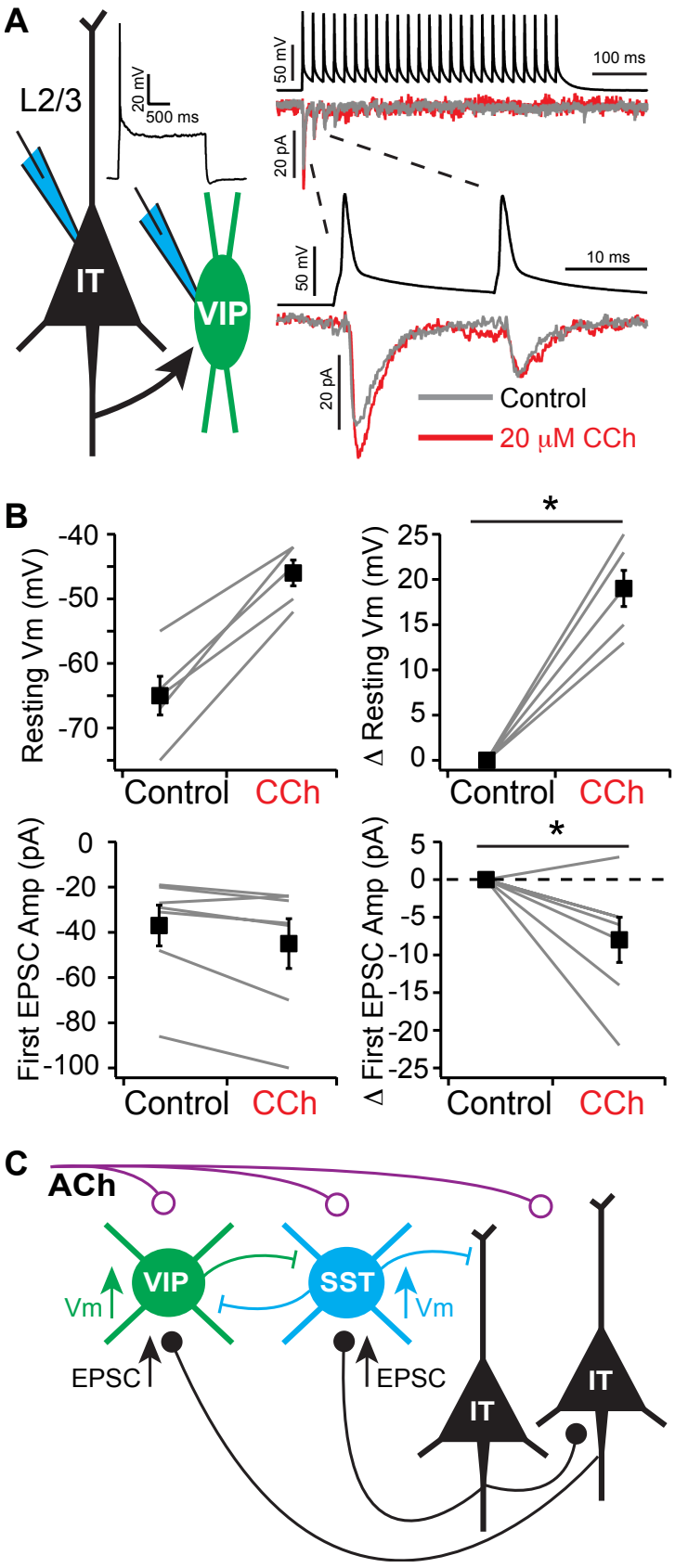

Figure S5. Related to Figure 4. Synaptic connections from IT PNs to VIP INs are potentiated by cholinergic modulation

A) Example IT PN to non-LS (fAD) IN synaptic connection (inset) in L2/3 before (gray) and after (red) wash-in of 20 μm carbachol (CCh). Postsynaptic currents are averages of 10 trials.

B) Raw (left) and normalized (right) resting Vm (n = 5 cells) and first postsynaptic response (n = 7 cells) before and after 20 μm carbachol (CCh) wash-in. * $p < 0.05$, Student's t-test.

C) Schematic depicting impact of cholinergic modulation on local circuit motifs involving VIP+ and SST+ INs in superficial cortical layers. VIP+ and SST+ IN membrane potentials (Vm) are depolarized and synaptic input from PNs is potentiated. ACh = acetylcholine.

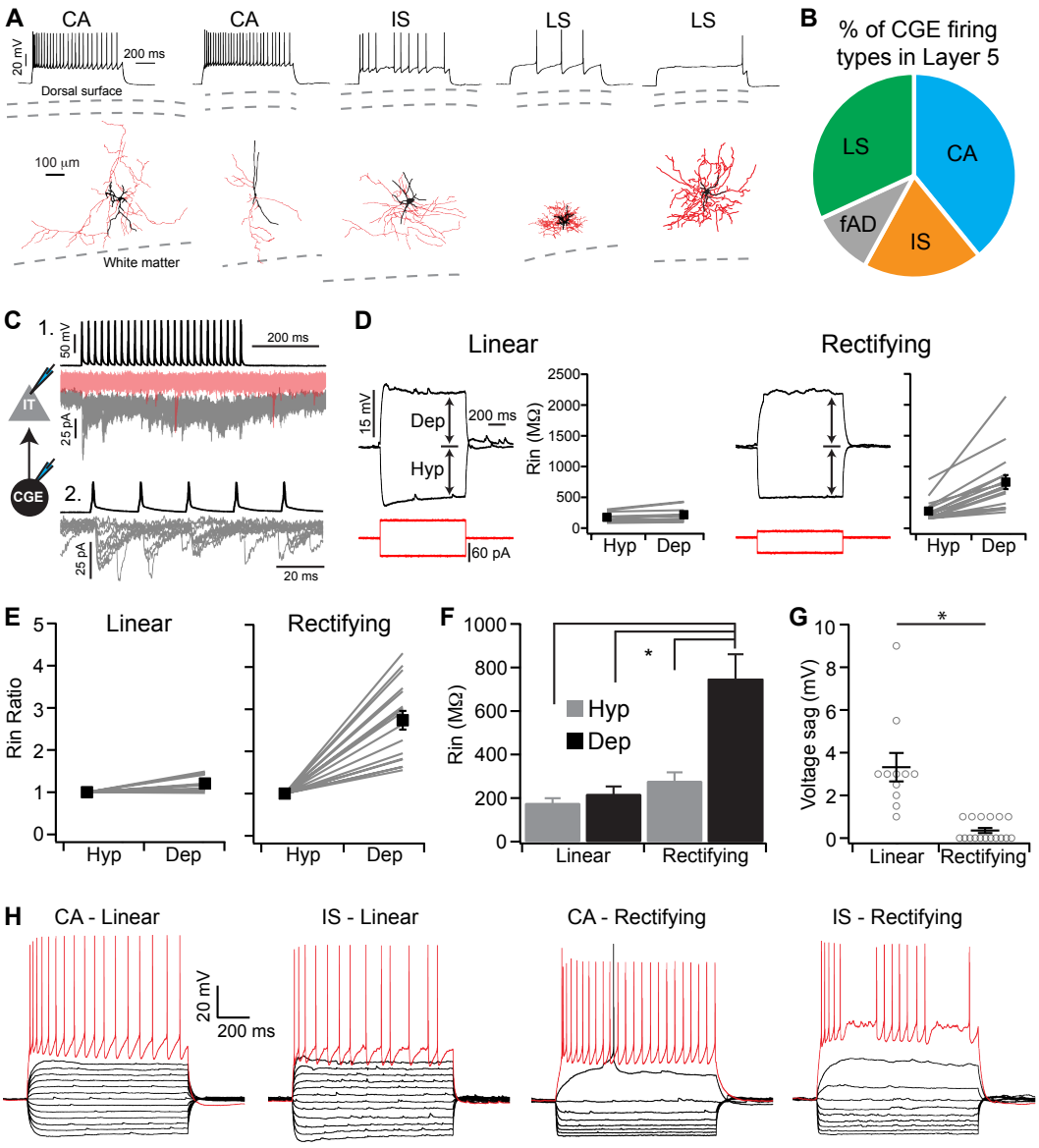

Figure S6. Related to Figure 5. Interneuron subtypes in deep cortical layers during paired recordings.

A) LS cells are likely reelin+ neurogliaform cells, while non-LS cells are heterogeneous morphologically but are likely VIP+ subtypes. CA, continuous adapting; IS, irregular spiking; fAD, fast adapting; LS, late spiking. Dendrites and soma are black and the axon is red.

B) Percentages of CGE-derived IN firing types found in deep layers of cortex in control mice (n = 69 cells). CA (39%), IS (19%), fAD (10%), LS (32%). CA, continuous adapting; IS, irregular spiking; fAD, fast adapting; LS, late spiking.

C) Examples of 5HT3A-GFP+ IN to IT-type PN synaptic connections. (1) LS INs provide weak input with asynchronous transmitter release that fades after multiple trials. (2) Non-LS IN (IS) input did not fade and was synchronous. Shown are 10 overlaid trials.

D) Analysis protocol to quantitatively parse the two subtypes of VIP+ INs. The input resistance was measured from membrane potential deflections from rest (-70 mV) in

depolarizing (+15 mV) or hyperpolarizing (-15 mV) directions. From these values, we calculated a ratio (E). 200 ms of steady-state membrane potential was used. Input resistance values from linear (n = 11) versus inward rectifying INs (n = 17).
E) Ratios calculated from (D). Linear INs were defined as having a ratio < 1.5.
F) Inward Rectifying INs are largely defined by significantly greater input resistance in response depolarizing pulses. * $p < 0.001$, Kruskal-Wallis test with post-hoc Dunn-Holland-Wolfe multiple comparisons test.
G) Linear INs (n = 11) have significantly greater voltage sag than inward rectifying INs (n = 17). * $p < 0.001$, Wilcoxon Rank test.
H) Linear versus inward rectifying membrane properties occur independent of firing type. CA, continuous adapting; IS, irregular spiking. Black traces are in response to constant amplitude current steps. Red traces are supra-threshold to demonstrate firing type.

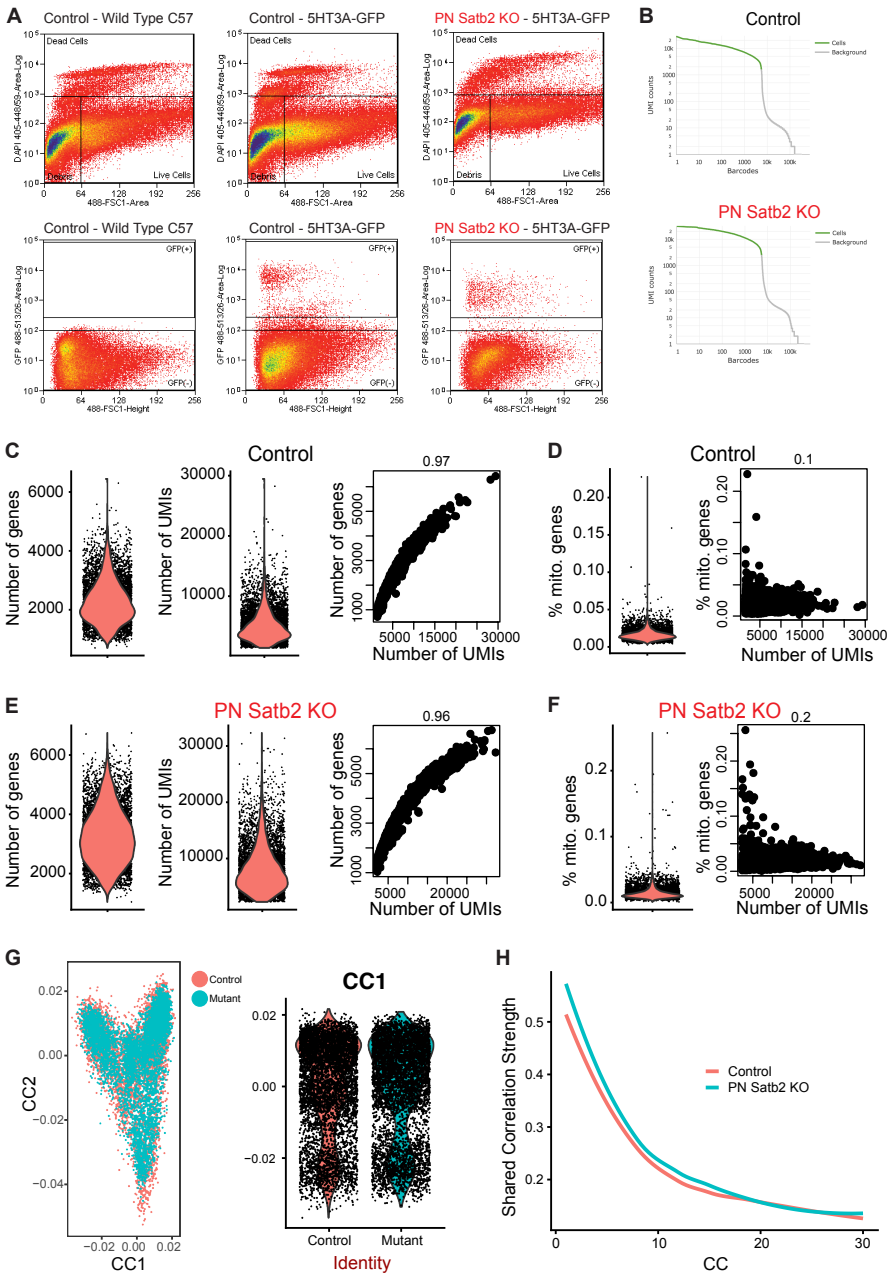

Figure S7. Related to Figures 7 and 8. Quality control data for single cell RNA-seq.

A) FACS plots showing gating for living GFP+ cells.

B) Barcode Rank Plots for INs from control and mutant mice, demonstrating separation of cell-associated barcodes and those associated with empty partitions. UMI = unique molecular identifier.

C) Distributions of the total number of genes and UMIs per cell in control mice and their Pearson correlation coefficient.

D) Percentage of mitochondrial genes detected in control mice. Subsequently filtered prior to secondary analysis.

E) Sames as (C) for mutant mice.

F) Same as for (D) for mutant mice.
G) Examples of canonical correlations used during integration and alignment of control and mutant datasets.
H) Shared correlation strength as a function of canonical correlation (CC) vectors. Based on drop-off, we used a limit of 30 CCs for integration and alignment of control and mutant datasets.

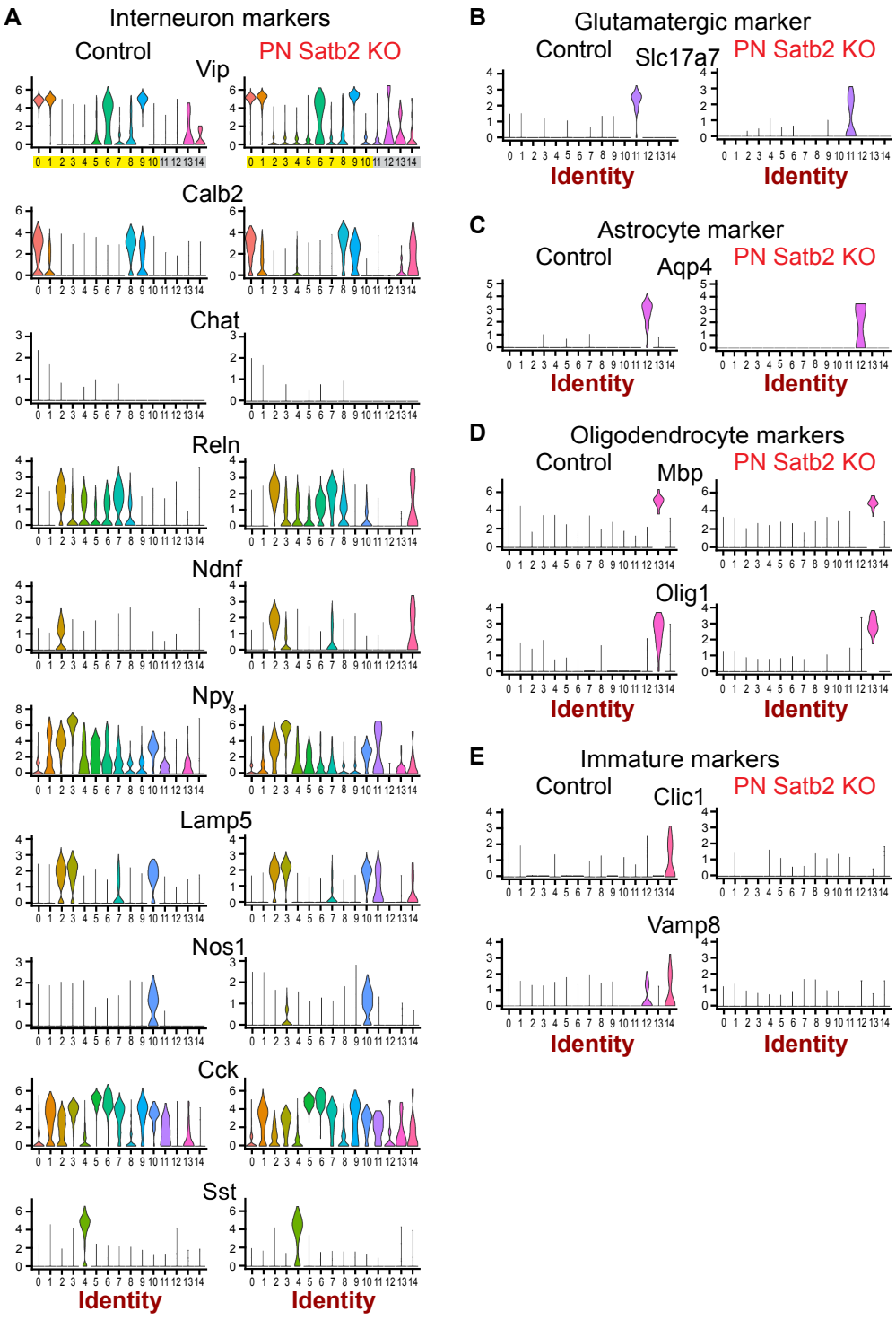

Figure S8. Related to Figures 7 and 8. Violin plots for expression of major molecular markers used to name clusters.

A) Transcription of major interneuron molecular markers used to identify clusters. Plotted is log gene expression as a function of cluster number. Yellow highlights Clusters 0 – 10, which were identified as interneurons. Gray highlights contaminant Clusters 11 – 14. Cluster identities from main text: Cluster 0 = VIP/CR/ChAT; Cluster 1

= VIP; Cluster 2 = Reelin/NDNF/Lamp5; Cluster 3 = NPY/Lamp5; Cluster 4 = SST; Cluster 5 = CCK;, Cluster 6 = CCK/VIP/Reelin; Cluster 7 = Reelin; Cluster 8 = CR; Cluster 9 = VIP/CR; Cluster 10 = nNOS/Lamp5; Cluster 11 = Glutamatergic; Cluster 12 = Astrocytes; Cluster 13 = Oligodendrocytes; Cluster 14 = Immature.
B) – E) Identification of small contaminant clusters by gene expression.

10X Genomics Cell Ranger Run Summaries		
	Control	PN Satb2 KO
Cells		
Estimated number of cells	5,565	5,405
Fraction reads in cells	95.0%	93.5%
Mean reads per cell	35,295	37,008
Median genes per cell	2,170	3,181
Total genes detected	21,746	22,667
Median UMI counts per cell	4,486	7,256
Sequencing		
Number of reads	196,420,794	200,029,072
Valid barcodes	97.1%	97.0%
Sequencing saturation	68.5%	48.7%
Q30 bases in barcode	94.9%	94.9%
Q30 bases in RNA read	79.9%	81.9%
Q30 bases in sample index	93.9%	93.9%
Q30 bases in UMI	95.4%	95.4%
Mapping		
Reads mapped to genome	91.3%	92.4%
Reads mapped confidently to genome	85.1%	87.1%
Reads mapped confidently to intergenic regions	5.7%	5.9%
Reads mapped confidently to intronic regions	24.7%	29.4%
Reads mapped confidently to exonic regions	54.7%	51.8%
Reads mapped confidently to transcriptome	50.6%	48.1%
Reads mapped antisense to gene	2.5%	2.2%

Supplemental Table 1. 10X Genomics Cell Ranger run summaries, Related to Figures 7 and 8.
Summary metrics and analysis results from the 10X Genomics Chromium analysis pipeline.

Selected significant differential gene expression						
			Log fold change of Avg Expression	% Mutant cells	% Control cells	Adjusted p value
Interneuron cluster	**Gene**					
VIP/CR/ChAT	Gria1	↑	0.316847102	0.549	0.243	8.25211E-23
	Grin2b	↑	0.465705204	0.903	0.622	2.99855E-39
	Cadm2	↓	-0.254290961	0.623	0.62	0.004204461
	Erbb4	↑	0.443073136	0.854	0.537	1.04453E-32
VIP	Gria1	↑	0.391367085	0.689	0.386	4.9804E-26
	Grin1	↑	0.285827827	0.469	0.239	2.42372E-14
	Grin2b	↑	0.402929861	0.732	0.433	6.0726E-26
	Prox1	↑	0.334035406	0.839	0.586	2.64021E-19
	Cadm2	↓	-0.590996129	0.571	0.737	5.71108E-33
	Erbb4	↑	0.45552498	0.876	0.614	3.25147E-37
Reelin/NDNF/Lamp5	Gria1	↑	0.413424241	0.658	0.314	2.52559E-19
	Gria4	↑	0.413693294	0.613	0.204	1.41146E-28
	Grin2a	↑	0.350241049	0.488	0.152	2.07304E-22
	Cxcl14	↓	-0.861958711	0.478	0.677	1.43713E-14
	Erbb4	↑	0.272557777	0.945	0.828	9.4819E-10
NPY/Lamp5	Gria1	↑	0.369368668	0.645	0.294	4.64474E-20
	Gria4	↑	0.454285707	0.614	0.221	1.28801E-28
	Grin2a	↑	0.352314467	0.593	0.258	1.24968E-18
	Grin2b	↑	0.378444037	0.906	0.671	2.21843E-20
	Prox1	↑	0.315528441	0.717	0.432	2.6064E-12
	Erbb4	↑	0.331069604	0.897	0.679	7.47211E-12
CCK	Gria4	↑	0.256471494	0.554	0.218	1.12114E-14
	Grin2b	↑	0.531281234	0.954	0.693	9.05082E-38
CCK/VIP/Reelin	Gria1	↑	0.330776853	0.865	0.543	1.24563E-12
	Grin2b	↑	0.482569682	0.937	0.61	5.33462E-24
	Cxcl14	↓	-0.268036607	1	0.997	4.85722E-06
	Prox1	↑	0.272054887	0.919	0.721	6.53715E-07
	Cadm2	↓	-0.319729641	0.81	0.75	0.019301729
	Erbb4	↑	0.325412612	0.917	0.672	1.59141E-12
Reelin	Gria1	↑	0.401887377	0.52	0.181	4.79328E-16
	Gria2	↑	0.262580479	0.931	0.789	8.50935E-06
	Grin2b	↑	0.393157101	0.912	0.649	8.12579E-13
	Cxcl14	↓	-0.390928748	0.964	0.963	2.39262E-18
	Prox1	↑	0.282440112	0.66	0.401	1.69715E-06
	Erbb4	↑	0.293869247	0.948	0.808	3.16883E-09
CR	Gria1	↑	0.37183528	0.579	0.263	1.7312E-08

	Grin2b	↑	0.469116733	0.772	0.433	8.79654E-12
	Cxcl14	↓	-0.774081494	0.755	0.933	9.53192E-23
	CCk	↑	0.338769757	0.488	0.27	0.002840969
	Reln	↑	0.350996229	0.634	0.403	0.028405896
	Cadm2	↓	-0.453157678	0.705	0.767	3.23321E-08
	Erbb4	↑	0.276852084	0.851	0.583	0.000114015
VIP/CR	Gria1	↑	0.275087627	0.639	0.37	0.001988546
	Grin1	↑	0.292852976	0.575	0.291	6.78405E-05
	Grin2b	↑	0.538843123	0.889	0.51	8.51306E-17
	Prox1	↑	0.257064109	0.871	0.533	0.000308109
	Erbb4	↑	0.48923618	0.939	0.684	4.6729E-17
nNOS/Lamp5	Gria1	↑	0.482611315	0.969	0.783	1.34357E-07
	Grin2a	↑	0.398617409	0.649	0.226	2.62559E-05
	Erbb4	↑	0.355497701	0.969	0.849	0.001085805

Supplemental Table 2. Selected significant differential gene expression, Related to Figures 7 and 8.
Differential gene expression analysis for specific transcripts referenced in the main text.

Supplemental Table 3. Complete differential gene expression analysis, Related to Figures 7 and 8.
Full output of the differential gene expression analysis within each identified cluster. Included as an Excel spreadsheet.